Theoretical Notes
Note 174

SC-RR-72 0400

IONOSPHERIC MODIFICATION OF THE ELECTROMAGNETIC PULSE FROM NUCLEAR EXPLOSIONS

R. D. Jones
Testing Technology Department

and

D. Z. Ring
Space Systems Department

Sandia Laboratories
Albuquerque, New Mexico
87115

July 1972

ABSTRACT

Dispersive effects of the ionosphere impose constraints on satellite electromagnetic pulse (EMP) sensors for nuclear explosion detection. Dispersion is more effective than absorption in reducing the EMP hazard to soft low-altitude satellites. In this report, an estimate of the EMP in the time domain is obtained by convolving a truncated Fourier series approximation of the source signal with the impulse response function of the ionosphere.

Key words: Ionosphere, EMP, dispersion

TABLE OF CONTENTS

IONOSPHERIC MODIFICATION OF THE ELECTROMAGNETIC PULSE FROM NUCLEAR EXPLOSIONS

INTRODUCTION

The most intense high-frequency electromagnetic pulse (EMP) from a nuclear explosion results from the turning of the gamma ray-produced Compton electrons by the geomagnetic field. The radiated signal consists of a pronounced single pulse of a few shakes duration followed by a low-amplitude tail lasting several microseconds. Superimposed on this low-amplitude tail are long-duration contributions resulting from air or ground asymmetry effects. By the time these components develop, however, the geomagnetic pulse is largely completed.

As the pulse travels it undergoes changes, depending on the electrical propertie of the medium through which it propagates. Because the ionosphere reflects back to earth EM field components below a nominal 10 MHz, and because the ionosphere partially absorbs those components above 10 MHz that are transmitted, the appearance of the pulse must change. However, the pulse waveform is more significantly affected by the dispersive characteristics of the ionosphere; i. e., phase and group velocities of the signal components vary with frequency. Therefore, substantial changes in the spectrum of the EM pulse propagated through the ionosphere would be expected. This report is concerned with an approximate time history of the stretchec out and attenuated turning EMP after transionospheric propagation. Propagation of the lower-frequency components resulting from air or ground asymmetry effects is not considered because of the high-pass characteristics of the ionosphere.

Most of the papers in the literature relating to distortion of the envelope of a pulse of radio waves after ionospheric propagation are restricted to a consideration of quasi-monochromatic or impulsive-type sources. Examples of quasi-monochromatic pulses are the cutoff sinusoid discussed by Ginzberg[1] and the Gaussian-modulated pulse considered by Wait.[2] In each case most of the signal energy is contained in a very narrow spectral region centered at ω_o, the carrier frequency.

Dispersive effects of the ionosphere on the transmission of impulsive-type signals have been described by Sollfrey[3] and by Karzas and Latter.[4] Sollfrey discussed a delta-function pulse, a broad-band pulse the spectrum $A(\omega)$ of which can be considered to be constant over a narrow bandwidth. On the other hand, Karzas and Latter considered a source with a time dependence of the form

$$f(\tau) = K(1 + \tanh \alpha\tau) \exp[-\beta\tau], \tag{1}$$

where K and β vary with burst altitude, α is the gamma-ray rise time constant, and $\tau = t - r/c$ is the retarded time. The form of the signal after propagation through the ionosphere was found by the method of steepest descent on the assumption that the ionosphere had a constant electron density. However, of more relevance to the present paper is the study by Price et al.,[5] who spectrally decomposed the source signal and then used a stationary-phase (or saddle-point) analysis to obtain the form of the individual signal components after dispersive propagation. These components were reassembled prior to detection.

In the analysis which follows the geomagnetic (or turning) signal is first approximated by a function of finite duration, i.e., a bounded function that is identically zero outside an interval of finite length. The periodic extension of this function is then approximated by a truncated Fourier series. By this artifice the geomagnetic signal is represented by a finite series of cutoff sinusoids. An estimate of the dispersed signal is obtained by first considering separately the distortion resulting from propagation through a dispersive channel of the separate quasi-monochromatic components, then reassembling these components to obtain an estimate of the signal envelope. By characterizing the ionosphere in terms of a quadratic phase function the composite signal can be approximated by a sum of Fresnel integrals. The saddle-point analysis requires that the phase variation of the source signal be slow relative to that introduced by the ionosphere. This restriction is not applicable to the technique described here.

In order to simplify the analysis, the birefringent effect of the geomagnetic field is neglected and the amplitude function of the ionosphere is regarded as a constant over the frequency range of interest. In addition, the ionosphere is considered to be homogeneous and isotropic, and energy absorption from electron collisions in the ionosphere is not considered. Despite these simplifying assumptions, the salient features of dispersion theory are retained in that a source transient of a few shakes

duration is distorted in propagation and becomes a waveform which lasts for many microseconds and is significantly reduced in amplitude. In fact, the effect of dispersion is so pronounced compared with the effect of absorption that the additional complexity introduced by taking into account the conductivity of the ionosphere is not warranted.

As a consequence of the EMP degeneration, it appears that the EMP threat to soft low-altitude satellite systems is appreciable mitigated. Also, it may be concluded that the waveform is so radically altered by transionospheric propagation that broad-band techniques would probably be ineffectual for diagnostic studies which utilize EMP sensors aboard surveillance satellites.

EFFECT OF IONOSPHERIC PROPAGATION

After propagation through a dispersive medium characterized by the transfer function $F(\omega)$, the signal, on suppressing the spatial variation, is given by

$$e(\tau) = e_s(\tau) * \frac{1}{2\pi} \int_{-\infty}^{\infty} F(\omega) \exp\left[j\omega\tau\right] d\omega, \tag{2}$$

where $e_s(\tau)$ is the undispersed signal. It is understood that the undispersed signal is of duration T and, therefore, can be represented by its periodic extension

$$e_s(\lambda) = \sum_{k=-\infty}^{\infty} e_{s_o}(\lambda + kT), \tag{3}$$

where

$$e_{s_o}(\lambda) = e_s(\lambda)\left[U(\lambda) - U(\lambda - T)\right].$$

Then, by defining $\omega_o = 2\pi/T$, $e_s(\lambda)$ can be written in the form of a uniformly convergent Fourier series:

$$e_s(\lambda) = \sum_{-\infty}^{\infty} D_k \exp\left(jk\omega_o\lambda\right). \tag{4}$$

The Fourier coefficients are given by

$$D_k = \frac{1}{T}\int_0^T e_s(\lambda)\exp(-jk\omega_o\lambda)\,d\lambda . \tag{5}$$

Because $e_s(\lambda)$ has a finite mean squared value, it can be approximated by a truncated series which, by setting $c_k \angle \phi_k = 2D_k$, takes the real form[6]

$$e_s(\lambda) \approx c_o + \sum_{k=1}^{K} c_k \cos(k\omega_o\lambda + \phi_k). \tag{6}$$

The constant term, c_o, represents the mean value of the function and, because it represents a dc energy term which cannot be propagated, does not affect the overall pulse shape. Further, the appearance of such a dc term is merely a concomitant feature of the mathematics used, and not a physically realizable process. Deleting the constant term, the undispersed signal is obtained as

$$e_s(\tau) = \sum_{k=1}^{K} c_k \sin k\omega_o\tau \left[U\left(\tau - \frac{\phi_k T}{2\pi k} - \frac{T}{4k}\right) - U\left(\tau - \frac{\phi_k T}{2\pi k} - \frac{T}{4k} - T\right)\right], \tag{7}$$

which is recognized to be a sum of cutoff sinusoids.

From (4), the Fourier transform $E_s(\omega)$ of $e_s(\lambda)$ is the sequence of equidistant pulses

$$E_s(\omega) = 2\pi \sum_{-\infty}^{\infty} D_k \delta(\omega - k\omega_o) \tag{8}$$

distance ω_o apart. The effect of introducing the step functions in (3) is to broaden the spectrum in the neighborhood of $k\omega_o$; i. e., the cutoff sinusoids (7) are only quasi-monochromatic. In the vicinity of $k\omega_o = \omega_k$, the transfer function can be approximated by

$$F(\omega) \approx \left| F(\omega_k) \right| \exp\left[-j\Omega(\omega)\right] . \tag{9}$$

For simplicity, assume the amplitude function, $|F(\omega_k)|$, to be slowly varying compared with $\exp[-j\Omega(\omega)]$ in the neighborhood of ω_k and expanding $\Omega(\omega)$ in a Taylor series about ω_k, truncating the series beyond the term containing the second derivative,

$$\Omega(\omega) \approx \Omega(\omega_k) + (\omega - \omega_k)\,\Omega'(\omega_k) + \frac{1}{2}\left(\omega - \omega_k\right)^2 \Omega''(\omega_k). \tag{10}$$

If $|F(\omega_k)|$ is considered a constant, it can be shown that the impulse response of the ionosphere in the neighborhood of ω_k is given by[7]

$$f(t) \approx \frac{1-j}{2\pi}\,|F(\omega_k)|\,\exp\left\{j\left[\omega_k t - \Omega(\omega_k)\right]\right\}\sqrt{\frac{\pi}{\Omega''(\omega_k)}}\;\exp\left\{j\,\frac{\left[\Omega'(\omega_k) - t\right]^2}{2\Omega''(\omega_k)}\right\}. \tag{11}$$

The k-th term of the dispersed signal of obtained by convolving (7) with (11) is given by

$$e_k(\tau) \approx \frac{1-j}{2\pi}\,\sqrt{\frac{\pi}{\Omega''}}\,|F(\omega_k)|\,c_k\exp\left\{j\left[\omega_k\tau - \Omega(\omega_k)\right]\right\}\int_{\lambda_1}^{\lambda_2}\exp\left\{j\,\frac{(\Omega' - \lambda)^2}{2\Omega''}\right\}d\lambda, \tag{12}$$

with limits

$$\lambda_1 = \tau - \frac{\phi_k}{\omega_k} - \frac{T}{4k} \quad \text{and} \quad \lambda_2 = \tau - \frac{\phi_k}{\omega_k} - \frac{T}{4k} + T.$$

It is convenient to denote time, θ_k, measured from the arrival of the k-th signal component as

$$\theta_k = \tau - \frac{\phi_k}{\omega_k} - \frac{T}{4k} - \Omega'(\omega_k). \tag{13}$$

It should be noted that $\Omega'(\omega_k)$ is now identified as the harmonic steady-state group delay, i.e.,

$$\Omega'(\omega_k) = \frac{5.3 \times 10^{-6}}{\omega_k^2}\int \text{Nds (MKS)}, \tag{14}$$

where the integral is the total electron content (TEC) integrated over the propagation path.[8] From the form of (13), then, it is obvious that θ_k decreases as k increases, showing that the higher-frequency components arrive earlier, as should be expected.

By defining a characteristic time

$$T_k \equiv \sqrt{\pi \Omega''(\omega_k)} \quad , \tag{15}$$

where the dispersion, $\Omega''(\omega_k)$, is given by

$$\Omega''(\omega_k) = \frac{2}{\omega_k} \Omega'(\omega_k), \tag{16}$$

and setting

$$\frac{\Omega'(\omega_k) - \lambda}{2\Omega''(\omega_k)} = x, \tag{17}$$

the integral in (12) can be written

$$\int_{\lambda_1}^{\lambda_2} \exp\left\{ j \frac{(\Omega' - \lambda)^2}{2\Omega''} \right\} d\lambda = \int_{-\theta/T_k}^{(\theta)-(T)/T_k} \exp(j\pi x^2/2)\, dx, \tag{18}$$

which is recognized to be the complex Fresnel integral. Suppressing the carrier term, the envelope of the k-th component is obtained as

$$\left| e_k(\tau) \right| = \frac{1}{\sqrt{2}} \left| F(\omega_k) \right| c_k \left| F\left(\frac{T - \theta}{T_k}\right) + F\left(\frac{\theta}{T_k}\right) \right|. \tag{19}$$

THE DISPERSED ELECTROMAGNETIC PULSE

Rather than the time dependence given in (1), for convenient calculational purposes, we assume a time dependence of the form

$$f_o(\tau) = \left(\exp[-a\tau] - \exp[-b\tau] \right) U(\tau). \tag{20}$$

This function has the disadvantage that its derivative is not zero at $\tau = 0$; otherwise, it is well-behaved. The maximum occurs at

$$\tau_m = \frac{1}{b - a} \ln \frac{b}{a} . \tag{21}$$

Although it can be argued that the spectral energy partition associated with the difference of two exponentials may very well depart significantly, particularly at early times, from that of a more realistic representation of the geomagnetic signal, it is believed that the gross distortion caused by the ionosphere can be illustrated by an elementary function.

Following the sequence of arguments leading to Eq. (6), $f_o(\tau)$ may be approximated by the function

$$f_1(\tau) = \left[c_o + \sum_{k=1}^{K} c_k \cos \left(\omega_k \tau + \phi_k \right) \right] \cdot \left[U(\tau) - U(\tau - T) \right] , \tag{22}$$

where

$$c_o = \frac{1}{aT} \left(1 - \exp[-aT] \right) - \frac{1}{bT} \left(1 - \exp[-bt] \right), \tag{23}$$

$$c_k = \frac{2}{T} \left\{ \left[\left(\frac{-a}{a^2 + \omega_k^2} \right) \left(\exp[-aT] - 1 \right) + \left(\frac{b}{b^2 + \omega_k^2} \right) \left(\exp[-bT] - 1 \right) \right]^2 \right. \tag{24}$$

$$\left. + \left[\left(\frac{\omega_k}{a^2 + \omega_k^2} \right) \left(\exp[-aT] - 1 \right) - \left(\frac{\omega_k}{b^2 + \omega_k^2} \right) \left(\exp[-bT] - 1 \right) \right]^2 \right\}^{1/2} ,$$

and

$$\phi_k = \tan^{-1} \frac{\omega_k \left(b^2 + \omega_k^2 \right) \left(\exp[-aT] - 1 \right) - \omega_k \left(a^2 + \omega_k^2 \right) \left(\exp[-bT] - 1 \right)}{-a \left(b^2 + \omega_k^2 \right) \left(\exp[-aT] - 1 \right) + b \left(a^2 + \omega_k^2 \right) \left(\exp[-bT] - 1 \right)} . \tag{25}$$

As an exercise, a CDC 6600 digital computer was used to determine a number of values of T, a, and b, subject to an arbitrarily chosen criterion that

$$\int_o^T \left[f_1(\tau) \right]^2 d\tau \geq 0.9 \int_o^\infty \left[f_o(\tau) \right]^2 d\tau ; \tag{26}$$

i.e., that $f_1(t)$ must contain at least 90 percent of the integral energy content of $f_o(t)$. Standard Gaussian digital integration techniques were used. The parameter "T" was set at 1.0 arbitrary time units (there is no loss of generality), and values for "a" from $a = 1/T$ to $a = 10/T$ were tried in integral increments. For each choice of "a", there were 16 corresponding cases chosen for "b", ranging from $b = 1.5a$ to $b = 9.0a$, in increments of 0.5a. Physically, the choices of "a" corresponded to a series of pulses with increasingly sharp rises with increasing "a", while the corresponding choices of "b" within an "a" category produced increasingly sharp falls with increasing "b".

Of 160 cases integrated and approximated on the digital computer, 143 produced $f_1(\tau)$ with the required 90-percent total square integral content compared to the corresponding $f_o(\tau)$. Those cases in which $f_1(\tau)$ was not a valid approximation of $f_o(\tau)$ in the required sense were 16 cases of $a = 1/T$ and the single case of $a = 2/T$, $b = 1.5a$, all of which represent the lowest rising and decaying cases under consideration, and correspond poorly to waveforms usually associated with the EMP from a high-altitude burst. For all the 143 cases considered, it was discovered that suitable $f_1(\tau)$ could be obtained in all cases for $K \leq 6$. This implies mathematically that the Fourier series for $f_o(\tau)$ is rather rapidly convergent for the pulse shapes under consideration. As expected, the shorter and sharper the pulse shape, the more terms are required for a suitable $f_1(\tau)$ approximand.

Figure 1 illustrates a five-term approximand obtained by periodic extension for representative values of a, b, and T. The plot of amplitude versus time was generated on a Stromberg Datagraphix 4020 plotter. The pulse $f_o(\tau)$, less its average value, is represented by the plot symbol A, and the approximand, $f_1(\tau)$, with c_o suppressed, is represented by the plot symbol o. The square integral values for $f_o(\tau)$, $f_o(\tau)$ terminated at time T, and $f_1(\tau)$ are denoted at the bottom of the plot by "true energy," "app. energy," and "series energy," respectively. The suppressed value c_o is also labeled in addition to the number of terms used to create $f_1(\tau)$. It should be noted that, because $f_1(\tau)$ is periodic, it diverges markedly from $f_o(\tau)$ near $t = T$. For comparison purposes, Fig. 2 shows a ten-term approximation to the double pulse. It should also be noted that the peak amplitude of the approximand in Fig. 2 more closely approximates that of the original pulse.

At this point it is appropriate to comment on the specific values assigned to the parameters a, b, and T in Figs. 1 and 2. The time variation of the early portion of

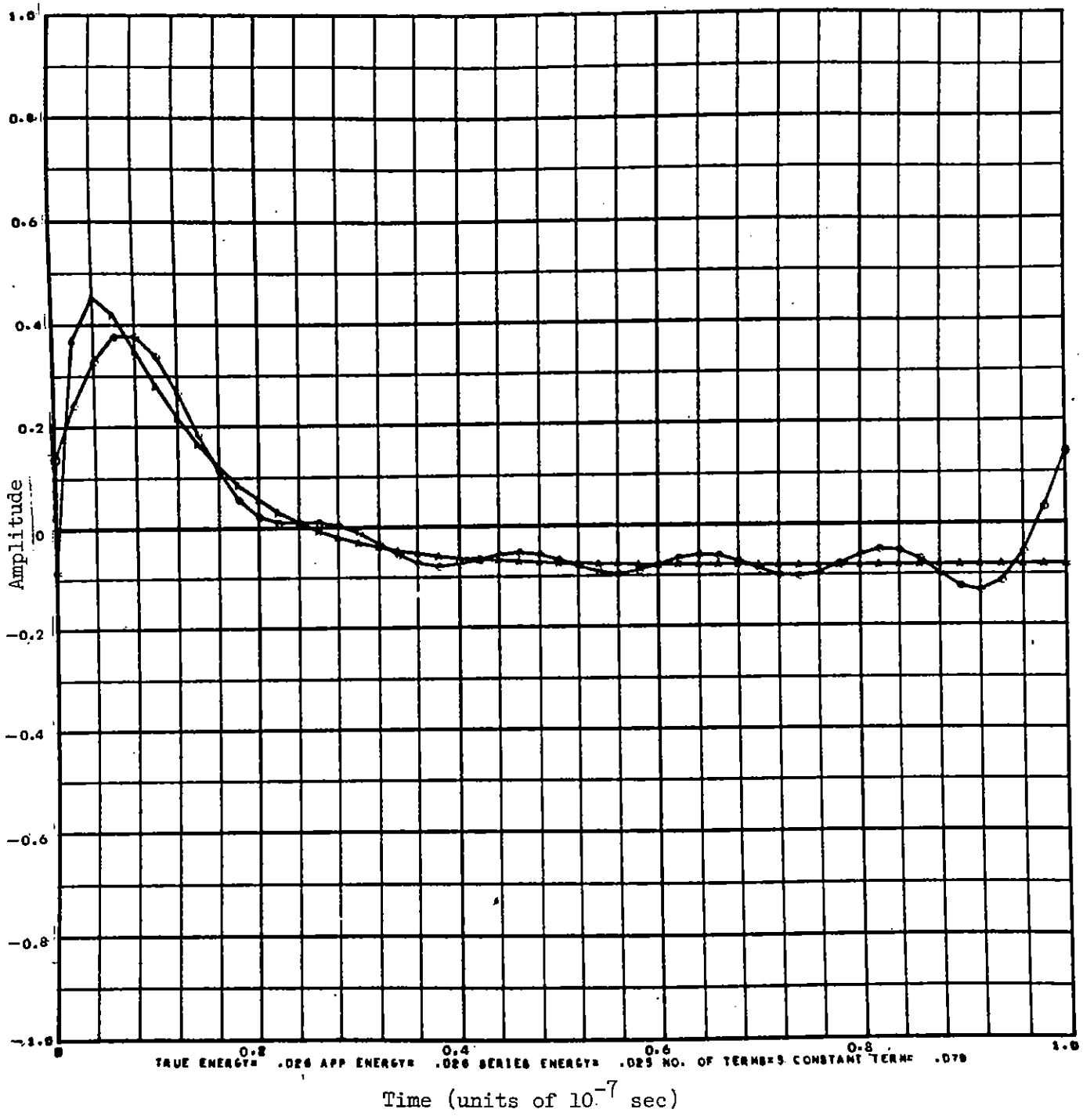

Fig. 1 Five-term approximation to a double exponential pulse.

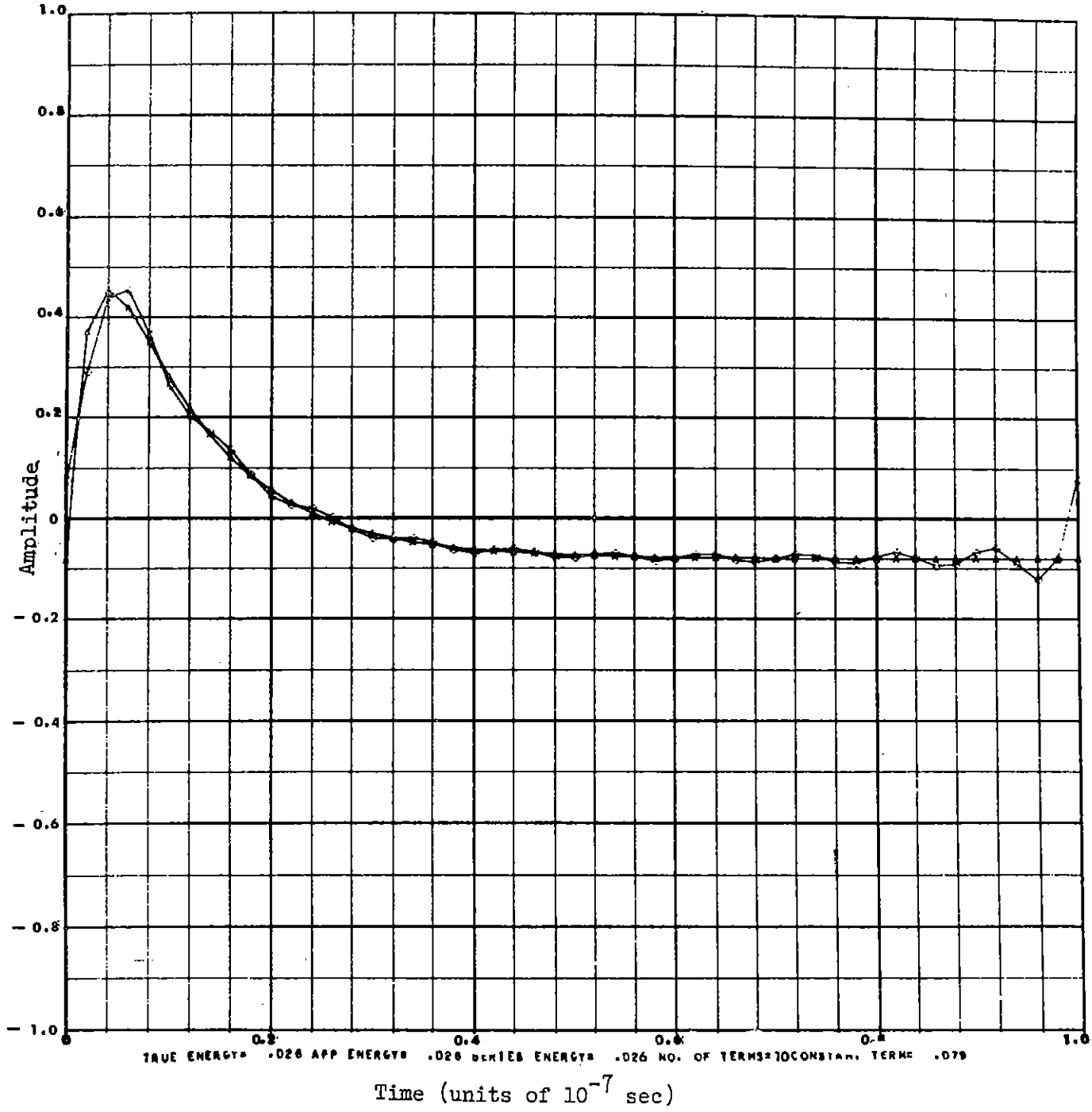

Fig. 2 Ten-term approximation to a double exponential pulse.

the electromagnetic signal from a low-altitude explosion is the same as that of the prompt gamma-ray emission. From (1) the signal rises as $\exp(\alpha t)$, where α is the gamma-ray rise time constant, and decays as $\exp(-\beta t)$ at late times. If $b \gg a$, then "a" dominates the decay rate. At low altitudes the signal decay time is related to the electron attachment rate to oxygen. For example, at sea level the lifetime of a 1.12-MeV Compton electron is about 8×10^{-9} sec. Therefore, it is reasonable to set $a \approx 10^{8}$ sec^{-1}. From (21) for $b = 5a$, the maximum signal amplitude occurs at 0.4×10^{-8} sec. The corresponding value of α, where an $\exp(\alpha t)$ type initial rise in signal amplitude is assumed, is roughly 4×10^{8} sec^{-1}.

The value assigned to T is not critical but, in order to satisfy (26), it must be at least 10a, in this case 10^{-7} sec. Therefore, the fundamental frequency component is 10 MHz, or 6.28×10^{7} rad sec^{-1}. However, only those signal components whose frequencies exceed the maximum plasma frequency (between 5 and 15 MHz) will be propagated through the ionosphere.[9] Because 10 MHz, the lowest frequency component, is near the ionosphere critical frequency, only terms of order greater than k = 1 will be retained.

Figures 3 through 6 show the enevelopes of the dispersed second through the fifth order cutoff sinusoids for a total electron content (TEC) of 10^{16} m^{-2}, a value not grossly atypical of an average ionosphere.* For convenience of calculation, $|F(\omega_k)|$ was taken to be unity. As expected, the distortion resulting from dispersion decreases as the order of the component increases.

Figure 7 shows a gross representation of the envelope of a five-term reconstituted pulse. Figure 8 shows the effect on the envelop resulting from inclusion of another five terms in the approximation. The additional high-frequency components are responsible for the shorter rise time to the peak amplitude (see Fig. 7). It should also be noted that the peak amplitude in Fig. 8 is greater than that of Fig. 7. This would be expected because of the better agreement between the ten-term approximation and the original pulse (see Fig. 2). However, in a comparison of Figs. 8 and 2, it can be observed that one effect of the ionosphere has been to decrease the peak amplitude by a factor of 6 (or 14 dB). Also the pulse duration (length of time for the amplitude to decrease to 1/e of its peak value) has been stretched out by a factor of roughly 130.

---

*The value of 10^{17} m^{-2} is commonly taken as typical of an average ionosphere and can vary by at least an order of magnitude in either direction, depending on time of day, season, position in the sunspot cycle, and direction of signal propagation.[8]

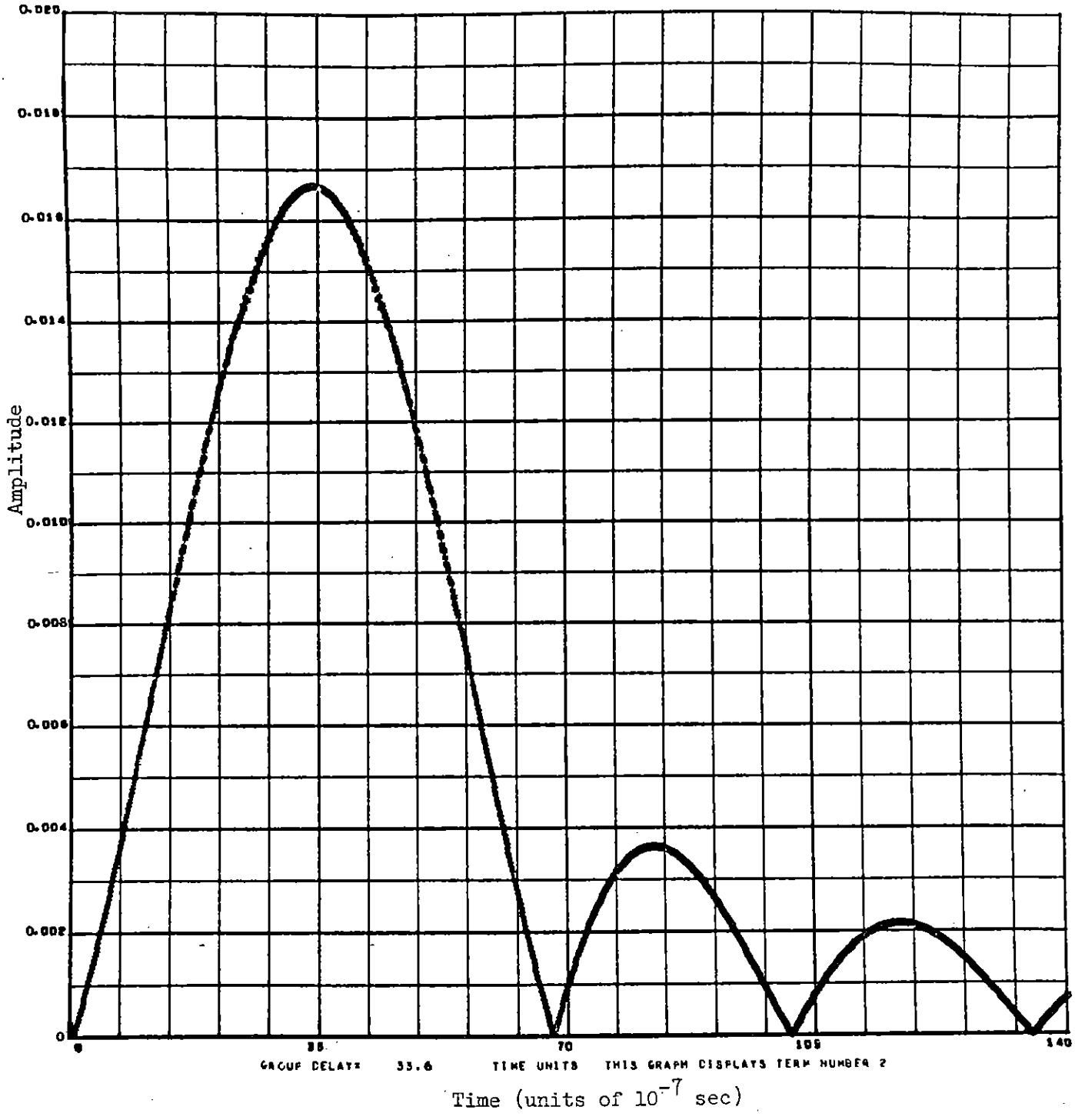

Fig. 3 Envelope of a dispersed second-order cutoff sinusoid (TEC = 1.0×10^{16} m^{-2}).

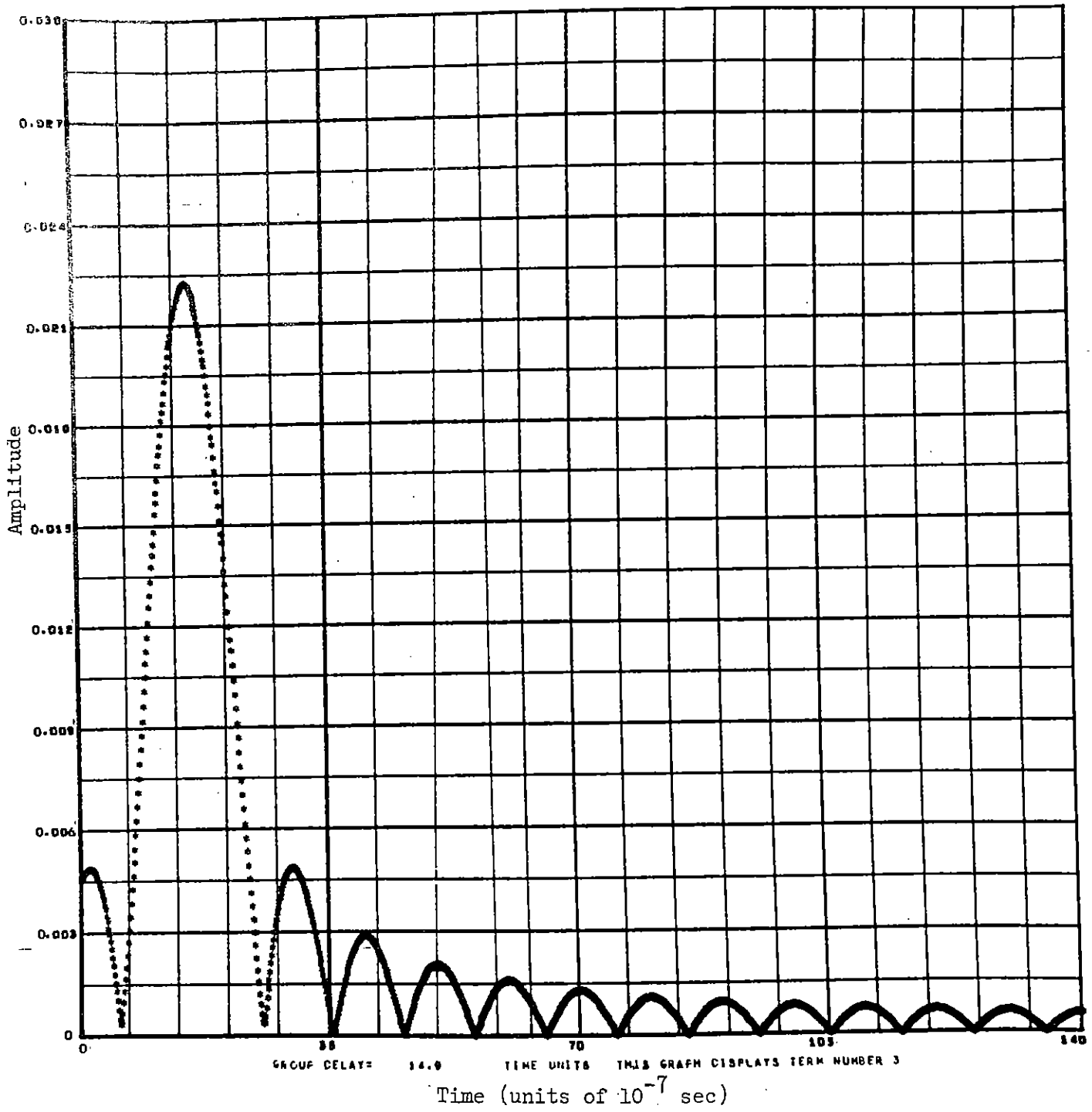

Fig. 4 Envelope of a dispersed third-order cutoff sinusoid (TEC = 1.0×10^{16} m^{-2}).

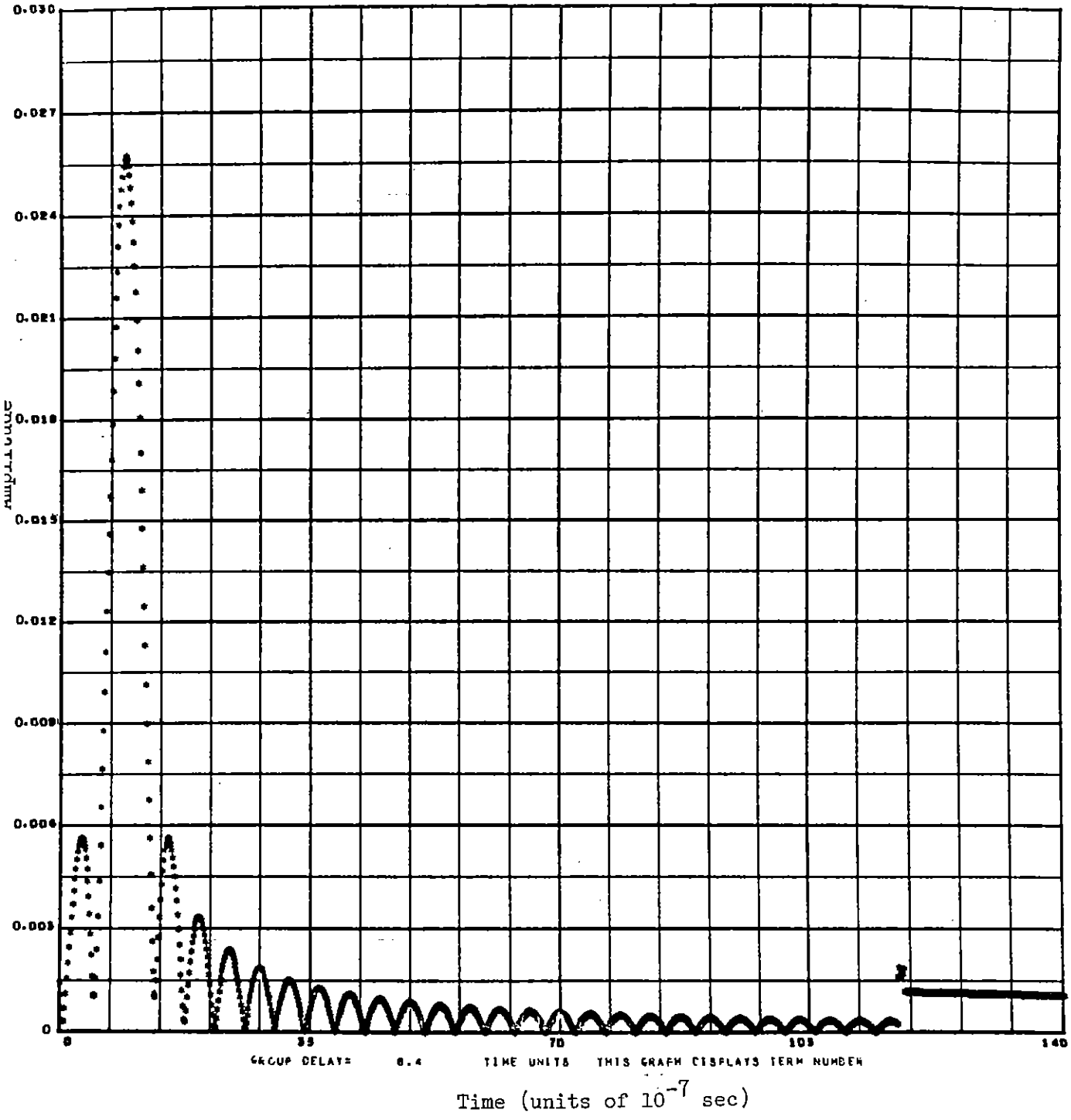

Fig. 5 Envelope of a dispersed fourth-order cutoff sinusoid (TEC = 1.0×10^{16} m^{-2}).

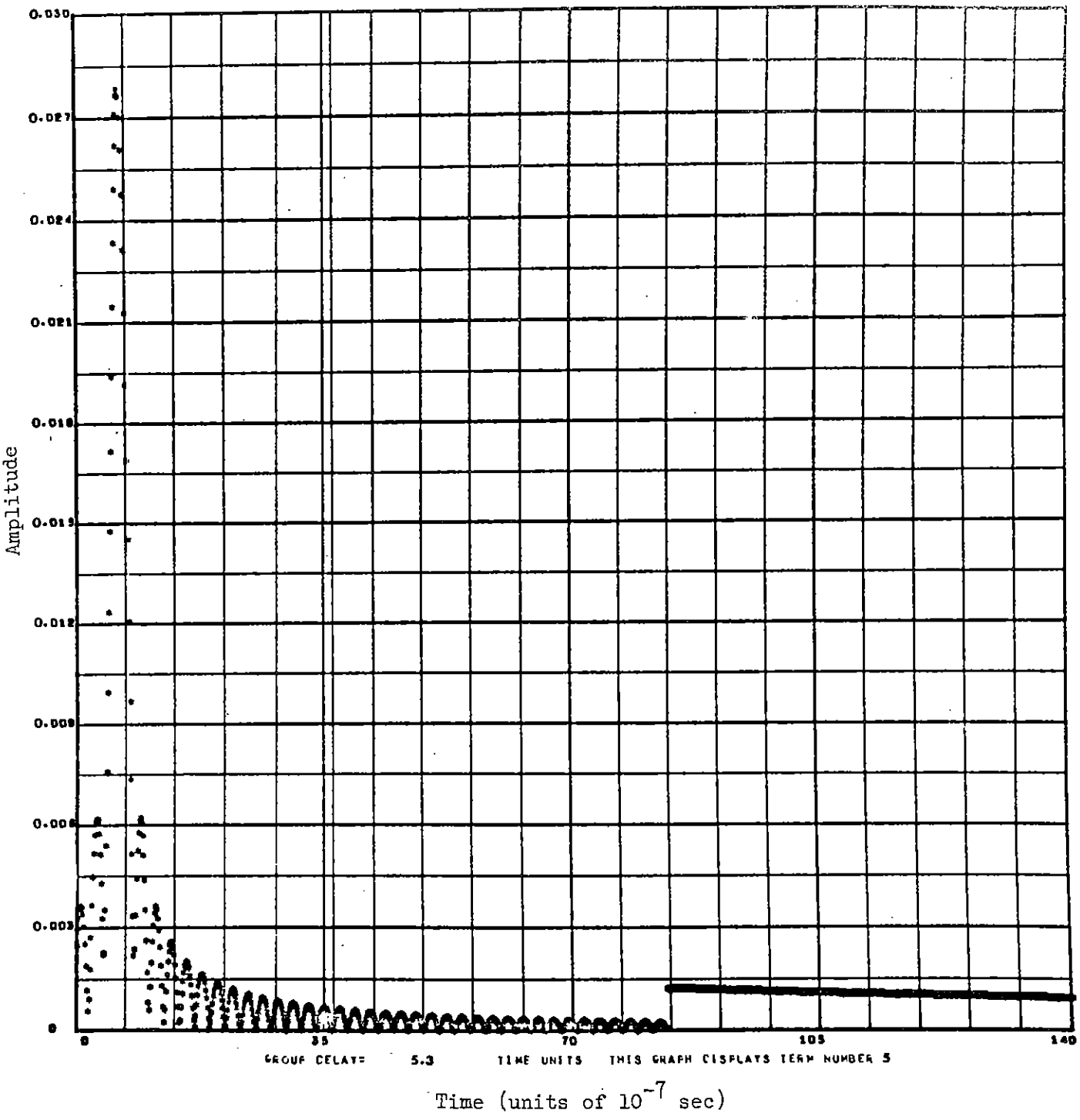

Fig. 6 Envelope of a dispersed fifth-order cutoff sinusoid (TEC = 1.0×10^{16} m^{-2}).

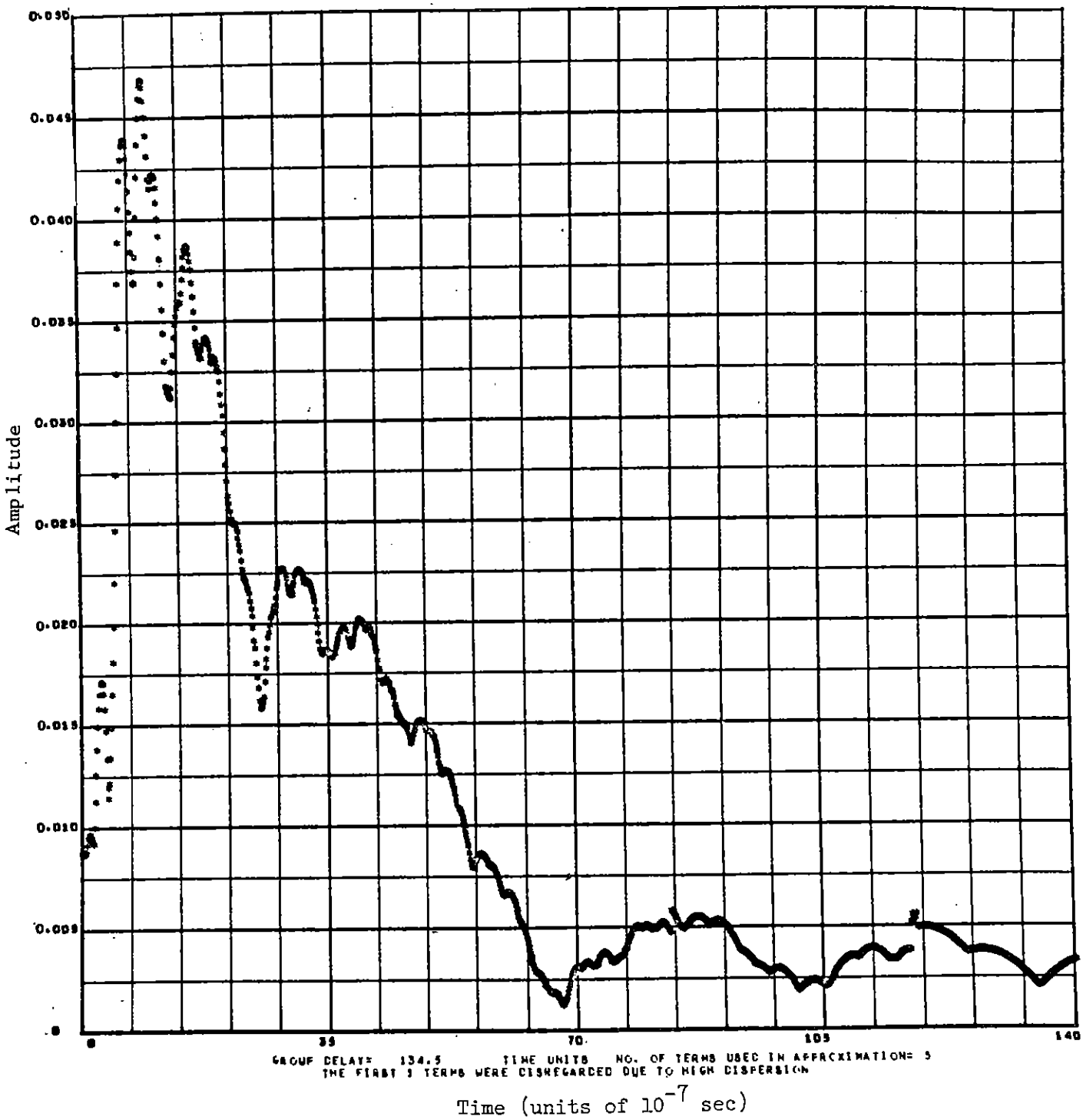

Fig. 7 Five-term approximation to a dispersed EMP (TEC = 1.0×10^{16} m^{-2}).

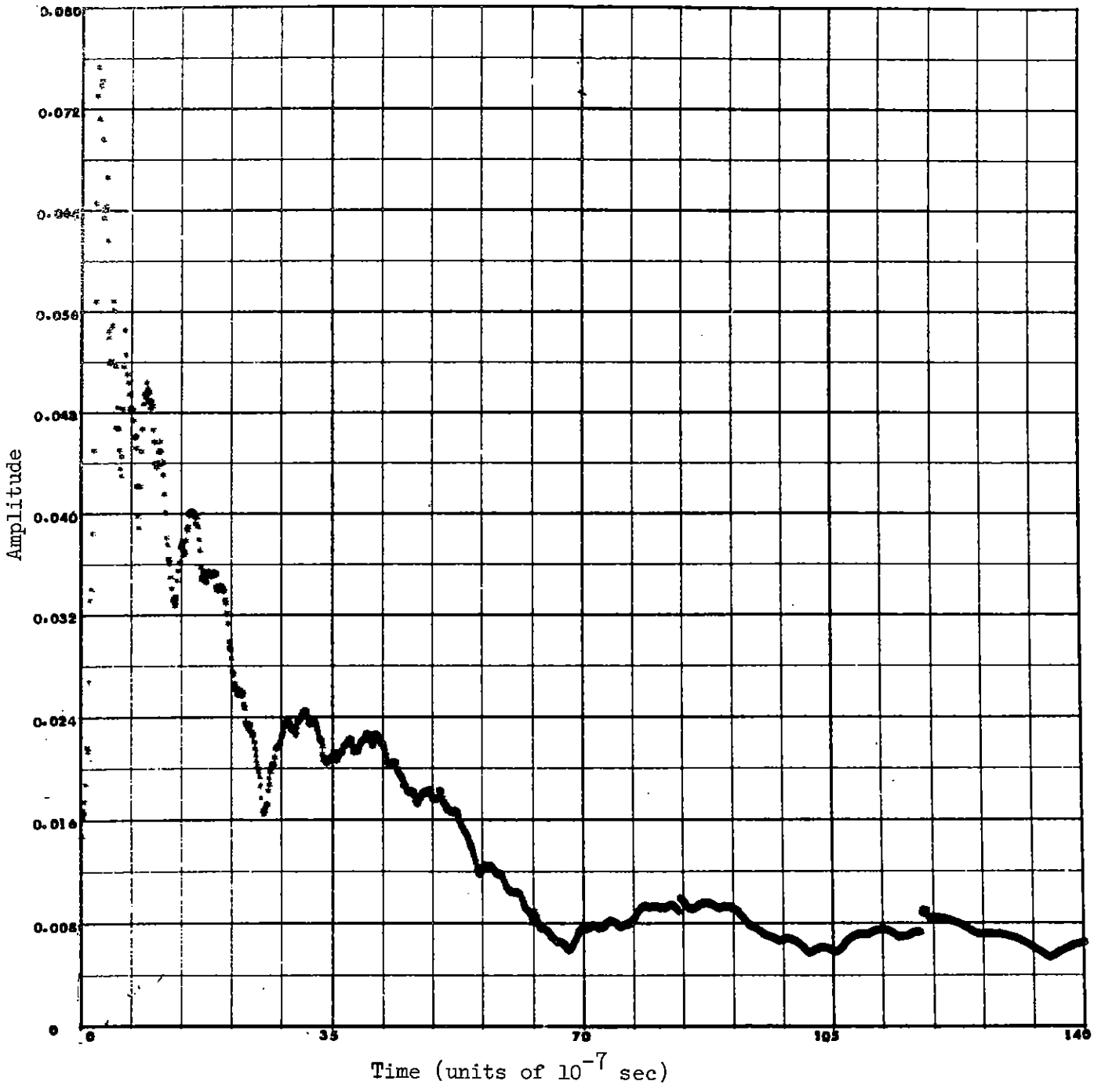

Fig. 8 Ten-term approximation to a dispersed EMP (TEC = 1.0×10^{16} m^{-2}).

Because the absorption of VHF components normally occurs in a region where ω is large compared with ν, the collision frequency, and $\omega \gg \omega_H$, where ω_H is the Larmor frequency, the absorption in decibels may be written[8] as

$$A = \frac{4.6 \times 10^{-5}}{\omega^2} \int_0^s N\nu \, ds.$$

The absorption for a TEC of 10^{17} m^{-2} is of the order of 0.05 dB at 100 MHz and, of course, only 5 dB at 10 MHz because of the inverse square frequency dependence. Clearly, the reduction in amplitude due to absorption may be disregarded in comparison with the reduction in amplitude resulting from dispersion. Therefore, neglect of the ionospheric conductivity is justified.

APPLICATIONS OF THE ANALYSIS

The preceding analysis can be used to obtain estimates of the maximum EMP intensities in two distinct environmental problem areas of interest. One problem area concerns the EMP threat to soft close-in satellites; the other problem area has to do with nuclear explosion intelligence obtained from diagnostic measurements at synchronous (or higher) altitudes. With selection of a minimum altitude of 500 km, the preceding analysis is applicable to both problem areas, since the highest electron concentrations occur below this altitude. Further simplification results by the assumption of a geometry in which the line of sight from observer to explosion intersects the earth's magnetic field orthogonally; i.e., a plane wave is assumed with an electric field initially polarized perpendicular to the earth's magnetic field and which is propagating transversely to this field.

The ionosphere extends down to perhaps 50 km, with its various daytime regions denoted by the symbols D, E, F, and F_2. It has no well-defined upper boundary, but merges into the heliosphere, where neutral and ionized helium atoms are the principal constituents. For present purposes, the ionosphere can be represented as a uniform plasma slab, having the same density as the ionospheric peak density and the same total electron content as the true ionosphere. The daytime peak electron density occurs at an altitude of roughly 350 km in the F_2 region. A nominal value for an

electron density representative of average daytime conditions for midlatitudes with high solar activity is 10^{12} m^{-3}. The corresponding maximum plasma frequency f_N from the well-known relationship,

$$f_N \approx 9N_e^{1/2} \text{ [Hz - MKS]} ,$$

is 9 MHz. If we associate a TEC of 10^{17} m^{-2} with a peak electron density of 10^{12} m^{-3}, the slab thickness turns out to be 100 km, the slab extending roughly from 300 to 400 km. Figure 9 shows a gross representation of the envelope of a ten-term reconstituted pulse propagated through such a slab. In a comparison of Figs. 9 and 2, it can be observed that the pulse duration has been increased by at least a factor of 1600, and the peak amplitude of the pulse has been decreased roughly by a factor of 22. Clearly, the ionosphere provides a substantial altitude of the shielding (27 dB) for a satellite against EMP propagating through the ionosphere, where it is assumed, of course, that the satellite orbit is beyond the F_2 region.

An approximation to the absolute value of the maximum peak electric-field intensity at a distance r from the burst point is given by

$$E \sim kE_s r_s/r, \tag{27}$$

where k is the ratio of the peak amplitudes in Figs. 9 and 2, E_s is the saturated field in the conducting region in the vicinity of the burst, and r_s is the radius of the conducting region. For burst altitudes up to about 20 km, for which the gamma-ray mean free path is less than the atmospheric scale height, r_s is typically of the order of a few gamma-ray mean free paths.

For a low-altitude detonation, E_s is given by[4]

$$E_s = B_o \frac{\nu_c (\alpha + \beta)}{2\gamma q} \left(\frac{R}{c}\right)^2, \tag{28}$$

where B_o is the earth's magnetic field, ν_c is collision frequency for slow electrons in air, R is Compton electron range, γ is the electron relativistic mass factor, $q \approx 3 \times 10^4$ is the number of secondary electrons produced by each Compton electron, and α, β,

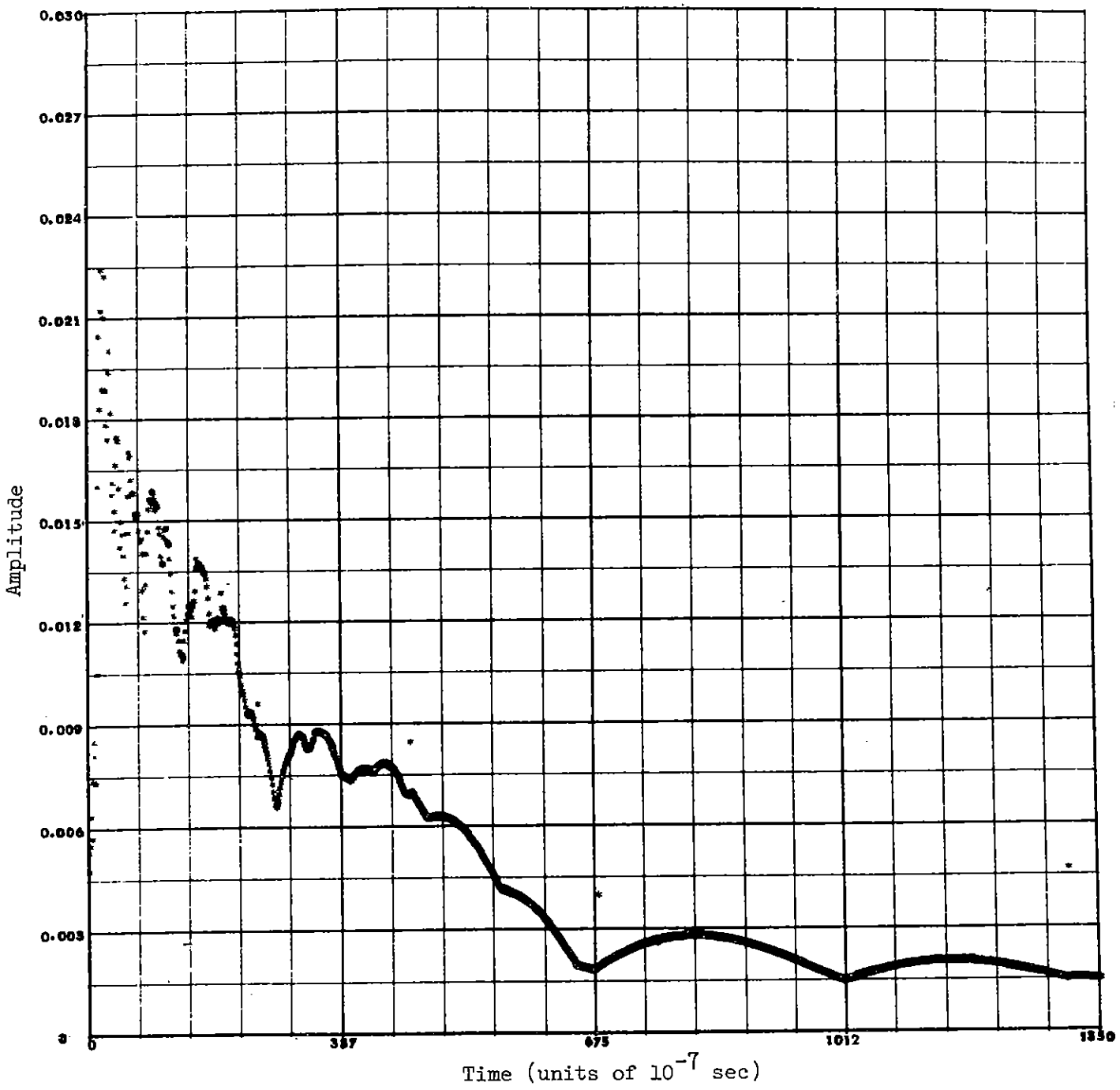

Fig. 9 Ten-term approximation to a dispersed EMP (TEC = 1.0×10^{17} m^{-2}).

and c are as defined earlier. As the altitude increases, E_s increases and the limiting value of E_s is attained at an altitude where the electron range is comparable to the Larmor radius. This value of E_s is given by[4]

$$E_s = \frac{m\omega_L \nu_c}{e\gamma q(1 - v/c)} \left(\frac{R}{c}\right), \tag{29}$$

where e is the charge on the electron and ω_L is the Larmor frequency, eB_o/m. By substituting appropriate values in (28) and (29), Karzas and Latter[4] obtain values of the peak electric field intensity in volts m^{-1} at a distance r km from the burst ranging from $10^3/r$ for a low-altitude explosion to about $10^6/r$ for the limiting high-altitude case.

A calculation of the peak EMP electric-field intensity in the environment of a satellite at, for example, 500 km altitude resulting from a nuclear burst at 100 km altitude is informative. To simplify the geometry, let us assume an earth-tangent, line-of-sight propagation path. Although the ray-path length is frequency-dependent, for present purposes a straight-line approximation will suffice. Also, we neglect the effect of the earth's magnetic field on propagation. For a low-altitude satellite at an altitude H, where H is very small compared to the radius of the earth, the slant range R to the horizon is given by

$$R \approx 110 \sqrt{H} \text{ km}. \tag{30}$$

It is assumed that the source of the signal is located in the first 500 km of the 3560-km path between the burst and the satellite. With Karzas and Latter's limiting value, the peak electric-field intensity for a nominal propagation path length of 3000 km is 330 volts m^{-1}. If the TEC along the propagation path is 10^{17} m^{-2}, the maximum electric-field intensity would be reduced to roughly 15 volts m^{-1}, a moderate field. However, for satellite altitudes below 500 km, spatial variation of ionization should be taken into account and the time history of the EMP recalculated for specific geometries of interest.

Examination of the dispersed waveforms shown in Figs. 8 and 9 leads to the conclusion that broadband techniques are unsuitable for diagnostic applications of exionospheric satellites. Significant episodes in the time history of a radioflash signal could be resolved, however, from narrow-band techniques (e.g., see Fig. 6

which typifies a receivable narrow-band signal). This, of course, reinforces a conclusion of Sollfrey[10] that, as the bandwidth of an EMP sensor increases, terms are added which are out of phase with the center of the band; the sensor may be regarded as "correlation-bandwidth limited."

Finally, in connection with analysis of data from the Vela 4 satellites,[11] it has been contended that the satellite suborbital point (the intersection of the earth's surface with the line joining the earth's center and the satellite) may, in some cases, be regarded as the origin of a signal source even though the earth-normal line has no significance for an omnidirectional sensor. The fact that dispersion tends to spread the signal energy over a longer period of time, thereby effectively reducing the peak amplitude, tends to suggest, in the case of weak EMP signals, that only those sources close to the suborbital point would be observable. Although the two optical path lengths from the satellite to the suborbital point and to the horizon of view may be almost equal, the difference in path length within the ionosphere may be as high as a factor of two for a horizon-source signal as compared with an earth-normal-source signal. Further, the increased electron content along oblique ray paths further increases the possibilities of signal incoherence, even within intermediate or narrow bandwidths. Thus, an apparent downward-looking location capability may be produced for an omnidirectional sensor. Exploitation of this effect for electromagnetic mapping of global thunderstorm activity and monitoring of man-made transmissions by simplified receiving systems on distant satellites are two possibilities suggested by this which are currently under investigation.

REFERENCES

1. Ginzburg, V. L., Propagation of Electromagnetic Waves in Plasma (Gordon and Breach, Science Publishers, Inc., New York, 1961) 411-423.

2. Wait, J. R., "On the optimum receiver bandwidth for propagated pulse signals," Proc. IEEE 57, 1784-1785 (1969).

3. Sollfrey, W., "Effects of propagation on the high-frequency electromagnetic radiation from low-altitude nuclear explosions," Proc. IEEE 53, 2035-2043 (1965).

4. Karzas, William J., and Latter, Richard, Satellite-Based Detection of the Electromagnetic Signal from Low and Intermediate Altitude Nuclear Explosions, Rand Corporation Memorandum RM-4542, June 1965.

5. Price, G. H., Carpenter, G. B., Nielson, D. L., and Watt, T. M., Stanford Research Institute Report (classified title), October 1970.

6. Javid, Monsour, and Brenner, Egon, Analysis, Transmission and Filtering of Signals (McGraw-Hill Book Co., Inc., New York, 1962), Chapter 2.

7. Jones, R. D., On Quasi-Monochromatic Signals Propagated through Dispersive Channels, SC-TM-70-516, Sandia Laboratories, July 1971.

8. Lawrence, R. S., Little, C. G., and Chivers, H. J. A., "A survey of ionospheric effects upon earth-space radio propagation," Proc. IEEE, 52, 1-27 (1964).

9. Mass, Jonathan, "Survey of Satellite Techniques for Studying Propagation," Radio Astronomical and Satellite Studies of the Atmosphere, Jules Aarons (Ed.) (North-Holland Publishing Co., Amsterdam, 1963) 256-288.

10. Sollfrey, W., Detection of High Frequency Electromagnetic Pulse Radiation from Nuclear Explosions, Rand Corporation Memorandum RM-4710 ARPA, October 1965.

11. Ring, D. Z., Measurement of VHF Earth-Produced Noise in the Exosphere, SC-TM-70-704, Sandia Laboratories, November 1970.